Organic Process Research & Development

ARTICLE

pubs.acs.org/OPRD

Design of Crystallization Processes for the Resolution of Conglomerate-Forming Chiral Compounds Exhibiting Oiling Out

Lorenzo Codan,[†] Matthäus Ulrich Bäbler,[‡] and Marco Mazzotti*[,†]

[†]Institute of Process Engineering, ETH Zurich, Sonneggstrasse 3, CH-8092 Zurich, Switzerland

[‡]Department of Chemical Engineering and Technology, KTH - Royal Institute of Technology, Teknikringen 36, SE-10044 Stockholm, Sweden

ABSTRACT: A methodology for the design of cooling crystallization processes for chiral resolution from nonracemic initial solutions is presented. Such processes are encountered when chiral resolution is attained by hybrid processes, where the crystallization step is preceded by a pre-enrichment step accomplished by either asymmetric synthesis or another separation technique. The work focuses on substances that crystallize as conglomerates and accounts for the occurrence of oiling out, i.e., an undesired liquid−liquid phase separation during crystallization. The generic ternary phase diagrams for conglomerate-forming systems with and without oiling out are derived. This knowledge is then applied to identify suitable operating conditions for chiral resolution. As crystallization is started from saturated solutions, the crystallization process is characterized by three parameters: the initial enantiomeric excess and the initial temperature, which together implicitly define the position of the operating point in the phase diagram, and the final operating temperature, which defines the composition and the amount of the phases present at the end of crystallization. For any initial enantiomeric excess, the methodology yields distinct areas in the initial versus final temperature plane containing pairs of operating temperatures that are suitable for chiral resolution. Such operating map bears great potential in improving the design and optimization of chiral resolution processes by crystallization.

1. INTRODUCTION

A high number of active pharmaceutical ingredients have a stereogenic center.[1] Because of the ability of living organisms to discriminate between enantiomers, the two enantiomers often do not have the same pharmacological effect. Several cases are known where the two enantiomers have a different therapeutic effect or differ in potency and toxicity.[2] Hence, the interest in the development of cost-efficient chiral separation techniques has rapidly increased in recent years under the pressure of new regulatory prescriptions.

Crystallization is a technique widely used to obtain substances of high chiral purity. Spontaneous resolution through direct crystallization from racemic solutions is however not possible. The formation of diastereomers[3] or the application of preferential crystallization[4] (only if the compound crystallizes as conglomerates) can overcome this limitation. Alternatively, the desired enantiomer can be obtained by selectively crystallizing it from an enriched feed solution by exploiting the equilibria involving enantiopure crystals of the target enantiomer and a less enriched liquid phase. The required pre-enrichment can be achieved through, e.g., asymmetric synthesis[5] or by an alternative separation technique upstream to crystallization such as simulated moving bed chromatography[6−10] or pertraction.[11]

In crystallization processes from enantiomerically enriched solutions, supersaturation can be created by cooling, i.e., crystallization starts from a saturated solution that is cooled to the final temperature where a favorable solid−liquid equilibrium can be exploited.

On the one hand, the yield increases as the system approaches the equilibrium state.[7] On the other hand, it increases by tuning the operating conditions, i.e., the final temperature of crystallization and the feed composition, so that the corresponding equilibrium involves a liquid phase with the lowest possible enrichment, i.e., the loss of target enantiomer in the equilibrium mother liquor is minimum. As a consequence, the crystallization process can be optimized on the basis of an accurate knowledge of the thermodynamic behavior of the ternary system involving the two enantiomers and the solvent from which the target enantiomer is crystallized,[12] complemented by measurements of kinetic data, e.g., nucleation and growth rates.[13,14]

The analysis of phase diagrams reveals that the lowest enrichment of a liquid phase that is at equilibrium with enantiopure crystals corresponds to the eutectic composition at the final crystallization temperature. However, in ternary systems, solid−liquid equilibria involving a eutectic liquid phase are not limited to a single temperature and can be obtained by either fixing the temperature and adapting the composition of the feed solution or vice versa. Hence, there are two ways to obtain the maximal recovery of the target enantiomer from the product stream delivered by the upstream process when we assume that the relative concentration of the two enantiomers, i.e., the enantiomeric excess, is fixed by the upstream process, either by leaving the composition of the feed stream unaltered and adapting the final operating temperature or by choosing the final operating temperature and adapting the composition of the feed solution by addition or removal of solvent. The choice is guided by the goal of minimizing the operational costs of the crystallization process without affecting the purity of the product, which is accomplished by comparing different crystallization operations at different

Special Issue: INTENANT

Received: July 18, 2011
Published: September 06, 2011

solvent concentrations of the feed solution (the enantiomeric enrichment of the feed solution is indeed fixed by the upstream process) and hence also at different operating temperatures.

Only few studies have addressed the determination of operating conditions that allow for chiral resolution over a wide temperature and composition range. Fung and Ng[15] have identified compartments in the liquidus projections of the ternary phase diagrams that contain operating points that allow for chiral resolution. Using solid−liquid equilibrium data, Kaspereit[16] determined operating conditions enabling the maximal recovery of the target enantiomer, which could be represented as curves in the initial versus final temperature plane for feed solutions of constant enantiomeric excess.

Some limitations in the choice of operating conditions are imposed by the occurrence of thermodynamically stable oiling out, which refers to the existence of liquid−liquid phase equilibria.[17] In the phase diagram the regions corresponding to these equilibria interfere in a disadvantageous manner with the ones of solid−liquid equilibria, which are favorable for chiral resolution. As oiling out yields impure crystals,[18] slows down growth,[19] and complicates process design and scale-up[19,20] the aim is to avoid the occurrence of oiling out during the crystallization process. This can be done by identifying operating conditions that allow conducting the crystallization process outside the region of oiling-out. To this aim a thorough understanding of the thermodynamic behavior of the system is essential. By identifying the new phase equilibria caused by the occurrence of oiling out, all possible generic polythermal phase diagrams can be derived, and using the information thereof a common methodology for the design of crystallization process can be developed.

In the first part of this work the thermodynamic behavior of conglomerate-forming systems is studied with the objective of deriving all possible generic polythermal phase diagrams. First the occurrence of oiling out is excluded, i.e., only solid−liquid equilibria are considered. Then a liquid−liquid phase separation region is introduced that intersects with the solid−liquid equilibria involving crystals of the pure enantiomers and extends over the whole enantiomeric composition range.

In the second part, a generalized methodology for the determination of suitable operating conditions for chiral resolution from partially resolved feed solutions is presented, based on the obtained generic polythermal phase diagrams. For any initial enantiomeric enrichment, the methodology yields domains in the initial versus final temperature plane containing operating temperatures that are suitable for chiral resolution. As the solute concentration of the feed solution is linked to the initial enantiomeric enrichment and to the initial temperature through solubility, the obtained areas implicitly represent all feasible feed compositions that can be attained by addition or removal of solvent from the product stream delivered by the process upstream crystallization.

2. GENERIC PHASE DIAGRAMS

2.1. Conglomerate-Forming Systems. *2.1.1. Thermodynamically Stable Multiphase Equilibria.* The phase diagram of a ternary system can be represented at constant pressure by a triangular prism with temperature as vertical axis. Assuming complete immiscibility in the solid phase and excluding the formation of polymorphs, only three solid phases, each composed of one of the three components, can be obtained from any ternary mixture. In the temperature range where solid−liquid equilibria

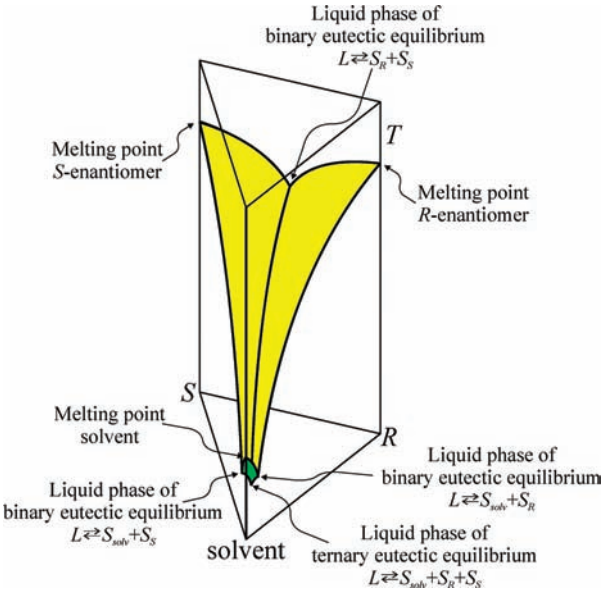

Figure 1. Schematic representation of the three liquidus surfaces of a ternary system forming conglomerates under the assumption of complete immiscibility in the solid phase and no formation of polymorphs. The yellow surfaces represent the solid−liquid equilibria comprising enantiopure solids, while the green surface describes the solid−liquid equilibria involving the solid solvent.

are thermodynamically stable, the equilibria among the individual solid phases and a liquid phase are represented by three liquidus surfaces that attain maximum temperature at the pure component vertex (Figure 1).[21] Where two liquidus surfaces intersect, a single liquid phase is at equilibrium with two different solid phases, thus forming a three-phase equilibrium, while the intersection of three liquidus surfaces leads to an equilibrium among four phases. Hence, beside the three solid−liquid equilibria, the three liquidus surfaces yield three solid−solid−liquid equilibria, one involving the two enantiopure solids, the other two involving the solid solvent and the solid *R*- or *S*-enantiomer, respectively, and a unique four-phase equilibrium comprising one liquid phase and the three pure components in the solid phase.

2.1.2. Temperature Range of Thermodynamic Stability of the Multiphase Equilibria. When increasing the temperature the first liquid phase from a three-phase solid−solid−solid system is formed through the ternary eutectic equilibrium $L \rightleftarrows S_{solv} + S_R + S_S$ corresponding to the intersection of the three liquidus surfaces. As the two liquidus surfaces of the two enantiomers are mirror images of each other, the emerging liquid phase *L* is of racemic composition. This is proven by demonstrating that the first liquid phase cannot be of nonracemic composition. If a nonracemic liquid phase were formed, system symmetry would require the concomitant appearance of another liquid phase equally enriched with the other enantiomer, thus forming an equilibrium comprising five phases, namely, two liquid and three solid phases, which would not comply with Gibbs phase rule applied to a three-component system at constant pressure.

Since the emerging liquid phase is at equilibrium with all solid phases, the temperature of the ternary eutectic equilibrium is the lowest temperature of thermodynamic stability among all possible multiphase equilibria. For all solid−liquid equilibria the corresponding highest temperatures are the melting points of the pure components. For the solid−solid−liquid equilibrium

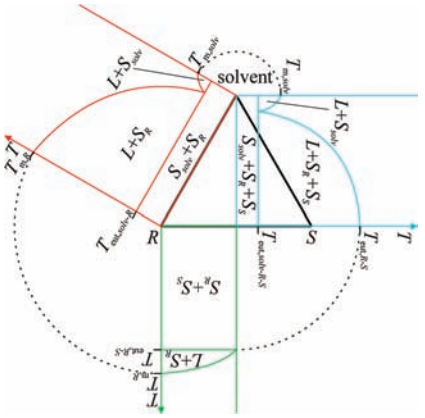

Figure 2. Eutectic and melting temperatures determining the topological evolution of the phase diagram of a ternary system forming conglomerates. The three polythermal cuts are turned down. The red one includes the *R*-enantiomer and the solvent; the blue one includes the racemic solid mixture and the solvent; the green phase diagram corresponds to a part of the binary phase diagram of the two enantiomers and is added only for the better understanding of the figure, as all the information it carries is contained in the first two polythermal cuts.

involving the two enantiopure solids, the highest temperature corresponds to the temperature of the binary eutectic equilibrium $L \rightleftarrows S_R + S_S$. For the solid−solid−liquid equilibria involving the solid solvent and one enantiopure solid, the highest temperature coincides with the temperatures of the two binary eutectic equilibria $L \rightleftarrows S_{solv} + S_R$ and $L \rightleftarrows S_{solv} + S_S$, which are identical due to symmetry. These two eutectic equilibria and the melting points of the solvent and of the pure enantiomers are found on the two polythermal cuts of the ternary phase diagram corresponding to the binary phase diagrams of pure enantiomer/solvent. Due to symmetry, the two polythermal cuts are identical, thus only one will be considered in the following. Furthermore, the liquid phases of the two eutectic equilibria $L \rightleftarrows S_R + S_S$ and $L \rightleftarrows S_{solv} + S_R + S_S$ are found on the polythermal cut characterized by an equimolar concentration of the two enantiomers (racemic composition). These two polythermal cuts, providing the temperatures of all eutectic equilibria and melting points, contain enough information to derive the temperature range of thermodynamic stability of all multiphase equilibria. In this particular case, the two polythermals cuts are two monoeutectic systems and are shown in Figure 2.

2.1.3. Generic Phase Diagrams. The knowledge of the temperature ranges of thermodynamic stability of all multiphase equilibria leads to a qualitative picture of the ternary phase diagram at any temperature. After identifying particular states and conditions on the polythermal ternary phase diagram that allow determining the temperature range of thermodynamic stability of all multiphase equilibria, constraining the position of these states by applying standard thermodynamic rules enables the determination of all possible types of ternary phase diagrams that fulfill the assumptions.

The conglomerate-forming behavior requires the melting temperature of the pure enantiomer $T_{m,R}$ to be higher than the temperature of the eutectic equilibrium $L \rightleftarrows S_R + S_S$, $T_{eut,R-S}$. Due to the eutectic character of the polythermal cuts, the temperature of the ternary eutectic equilibrium $L \rightleftarrows S_{solv} + S_R + S_S$, $T_{eut,solv-R-S}$, has to be lower than both the eutectic temperature $T_{eut,R-S}$ and the melting point of the solvent $T_{m,solv}$. The same

Table 1. Constraints Applicable to Eutectic and Melting Temperatures of Simple Conglomerate-Forming Systems

(1)	$T_{m,R} > T_{eut,R-S}$
(2)	$T_{eut,R-S} > T_{eut,solv-R-S}$
(3)	$T_{m,solv} > T_{eut,solv-R-S}$
(4)	$T_{m,R} > T_{eut,solv-R}$
(5)	$T_{m,solv} > T_{eut,solv-R}$
(6)	$T_{eut,solv-R} > T_{eut,solv-R-S}$

Table 2. Types of Conglomerate-Forming Systems Categorized by the Sequence of Eutectic and Melting Temperatures[a]

type I			$T_{m,solv}$	$T_{eut,R-S}$
type II		$T_{eut,solv-R}$		$T_{m,solv}$
type III	$T_{eut,solv-R-S}$		$T_{eut,R-S}$	$T_{m,R}$
type IV				$T_{m,solv}$
type V		$T_{eut,R-S}$	$T_{eut,solv-R}$	$T_{m,R}$

type I				$T_{m,R}$
type II			$T_{m,solv}$	
type III			$T_{m,R}$	$T_{m,solv}$
type IV			$T_{m,solv}$	$T_{m,R}$
type V			$T_{m,R}$	$T_{m,solv}$

[a] The temperature increases from left to right.

applies to the temperature of the binary eutectic equilibrium $L \rightleftarrows S_{solv} + S_R$, $T_{eut,solv-R}$, which has to be lower than the melting temperature of the pure enantiomer $T_{m,R}$ and of the pure solvent $T_{m,solv}$. The constraint $T_{eut,solv-R-S} < T_{eut,solv-R}$ follows from the fact that the first liquid phase emerging from a three-phase solid−solid−solid system is of racemic composition. The complete set of constraints is summarized in Table 1.

The number of generic ternary phase diagrams is finally obtained by permuting the order of the two eutectic and the three melting temperatures while accounting for the constraints mentioned above. The permutation yields five types of phase diagram, whose sequences of eutectic and melting temperatures are reported in Table 2.

2.1.4. Construction of Qualitative Ternary Phase Diagrams from Eutectic and Melting Temperatures. The construction of the ternary phase diagram using a specific sequence of eutectic and melting temperatures is exemplarily demonstrated for a system of type I. For this purpose, the ternary phase diagram of a system of this type was modeled using the ideal Schroeder−Van Laar equation:

$$\ln x_i = \frac{\Delta H_m(T_{m,i})}{R}\left(\frac{1}{T_{m,i}} - \frac{1}{T}\right) \quad (1)$$

where x_i is the mole fraction of component i in solution, and $T_{m,i}$ and $\Delta H_m(T_{m,i})$ are its melting temperature and melting enthalpy, respectively.[22] A selection of isothermal ternary phase diagrams at increasing temperature is shown in Figure 3. The six parameters used in the model to calculate the diagrams are listed in the figure caption.

According to Table 2, the first liquid phase emerges at the temperature of the ternary eutectic equilibrium $T_{eut,solv-R-S}$ (Figure 3a). The new liquid phase yields new phase equilibria with the pure solid phases, leading to three solid−solid−liquid equilibria and three solid−liquid equilibria right above $T_{eut,solv-R-S}$ (Figure 3b). Once the temperature of the first binary eutectic equilibrium $T_{eut,solv-R}$ is reached, a liquid phase will emerge along the binary diagram consisting of the pure enantiomer and the solvent. This corresponds to the temperature where the liquid region L reaches the sides of the phase triangle (Figure 3c); the two three-phase regions involving the solid solvent disappear at

dx.doi.org/10.1021/op200191d |*Org. Process Res. Dev.* 2012, 16, 294–310

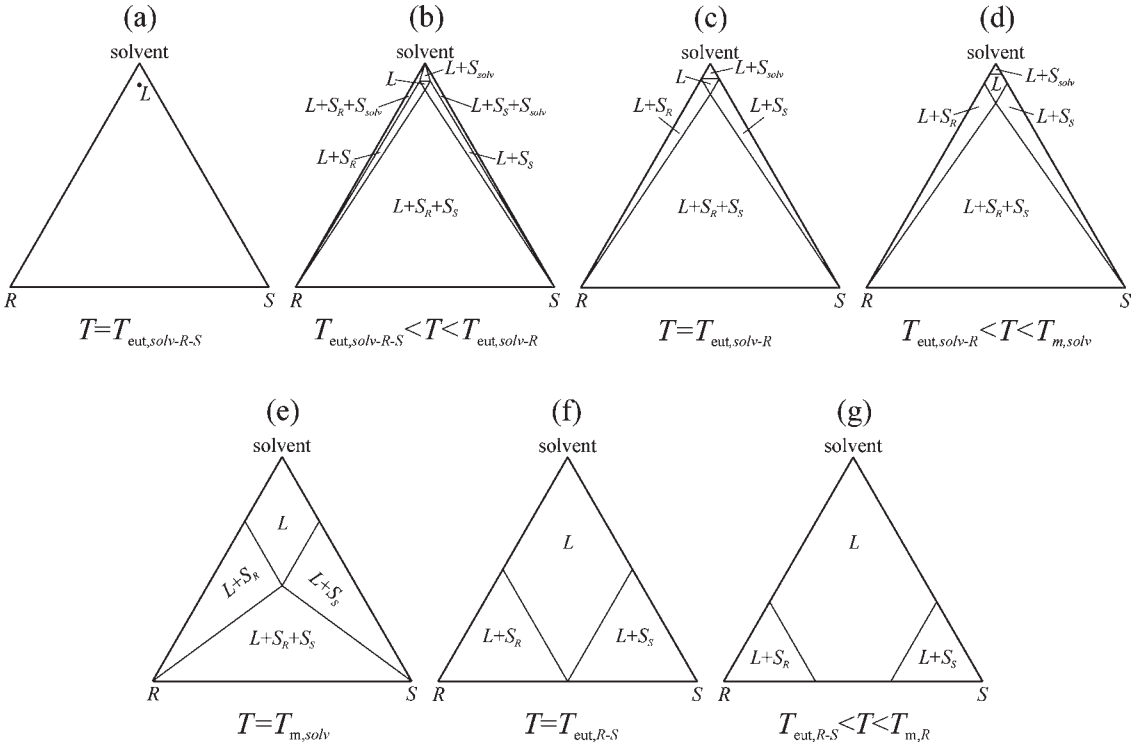

Figure 3. Evolution of the phase diagram of an ideal conglomerate-forming system of type I. Properties of the two enantiomers: $\Delta H_{m,R}$ = 29.6 kJ/mol, $T_{m,R}$ = 56 °C. Properties of the solvent: $\Delta H_{m,solv}$ = 2.6 kJ/mol, $T_{m,solv}$ = 7 °C. Key temperatures obtained from model: $T_{eut,solv-R-S}$ = − 15.9 °C, $T_{eut,solv-R}$ = − 9.3 °C, $T_{eut,R-S}$ = 36.2 °C.

this temperature. After going through an intermediate situation shown in Figure 3d, at the melting temperature of the solvent, $T_{m,solv}$, the solid−liquid phase region $L + S_{solv}$ disappears (Figure 3e). With increasing temperature, the solubility isotherms of the two remaining solid−liquid equilibria will move towards higher concentrations, and at $T_{eut,R-S}$ the intersection of the two solubility isotherms will reach the base of the triangle, thus leading to the disappearance of the solid−solid−liquid phase region $L + S_R + S_S$ (Figure 3f). Above these temperatures, the area of the two remaining solid−liquid phase regions (Figure 3g) will become smaller and smaller, until they disappear at the melting temperature of the pure enantiomers $T_{m,R}$.

In all five types of systems, the first liquid phase will emerge at $T_{eut,solv-R-S}$ and will lead to a phase diagram with the same number of phase regions as the one presented in Figure 3b. Increasing temperature causes the disappearance of the multiphase equilibria until reaching a ternary phase diagram consisting of one single liquid phase above the highest melting temperature of the system. The sequence of disappearance of the single phase regions is unequivocally defined by the sequence of the other eutectic temperatures and of the three melting temperatures.

2.2. Conglomerate-Forming Systems Exhibiting Oiling Out. *2.2.1. Thermodynamically Stable Multiphase Equilibria.* Following the same approach, consider conglomerate-forming systems exhibiting thermodynamically stable oiling out, under the assumptions of complete immiscibility in the solid phase and of lack of polymorphs. Regarding oiling out, we assume that the region of liquid−liquid phase separation extends over the entire range of enantiomeric compositions, and we restrict our discussion to cases where oiling out affects only solid−liquid equilibria involving crystals of the pure enantiomers. An example of a real system exhibiting such behavior has been reported earlier

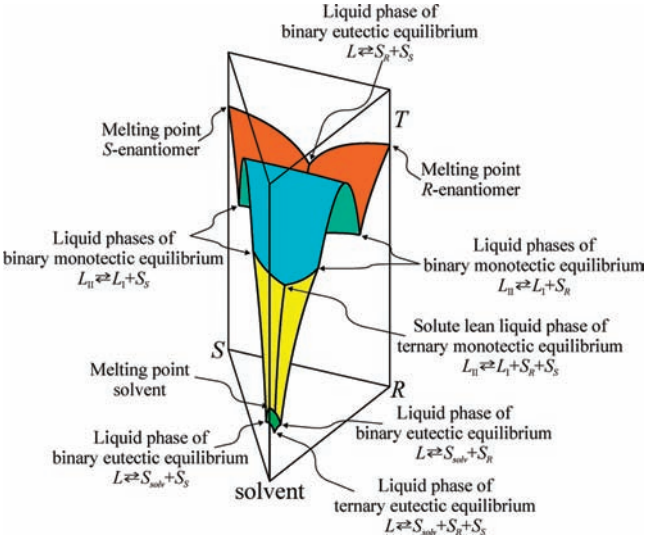

Figure 4. Schematic representation of the surfaces describing solid−liquid and liquid−liquid equilibria of a ternary system forming conglomerates exhibiting oiling out. The yellow and the orange surfaces represent the liquidus surfaces of the enantiopure solids, while the green surface describes the liquidus surface of the solvent. The blue surface represents the liquid−liquid equilibria.

where the complex phase behavior has been fully characterized experimentally.[17]

In the ternary phase diagram, schematically represented in Figure 4, oiling out manifests itself in the appearance of a new (blue) surface describing the liquid−liquid equilibria, which completely separates the lower (yellow) from the upper

dx.doi.org/10.1021/op200191d |*Org. Process Res. Dev.* 2012, 16, 294–310

(orange) liquidus surfaces describing the solid−liquid equilibria involving crystals of the pure enantiomers.

The six surfaces indicate the presence of six different two-phase equilibria, namely, five solid−liquid equilibria and one liquid−liquid equilibrium. Three solid−solid−liquid equilibria are generated by the pairwise intersections among the two lower liquidus surfaces of the pure enantiomers and the liquidus (green) surface of the solvent. Moreover, the concomitant (at the same temperature) intersections of the lower and the upper liquidus surfaces of each enantiomer with the solute-lean and the solute-rich part of the liquid−liquid equilibrium surface, respectively, generate two different solid−liquid−liquid equilibria. Finally, the intersection between the two upper liquidus surfaces creates another solid−solid−liquid equilibrium involving the two enantiopure solids. As for simple conglomerate-forming systems, the intersection of three liquidus surfaces, i.e., the lower liquidus surfaces of the two enantiomers and the liquidus surface of the solvent, creates a ternary eutectic equilibrium $L \rightleftarrows S_{solv} + S_R + S_S$. The concomitant intersection of the solute-lean part of the liquid−liquid equilibrium surface with the two lower liquidus surfaces and of the solute-rich part with the two upper liquidus surfaces yields a ternary monotectic equilibrium $L_{II} \rightleftarrows L_I + S_R + S_S$.[23]

2.2.2. Thermodynamic Stability of the Multiphase Equilibria. After the possible multiphase equilibria have been identified, their range of thermodynamic stability has to be determined. The temperature of the ternary eutectic equilibria $T_{eut,solv-R-S}$ corresponds to the lowest temperature of thermodynamic stability among all multiphase equilibria arising from intersections among the lower liquidus surfaces of the pure enantiomers and the liquidus surfaces of the solvent. We refer to Section 2.1.2 for the highest temperature of thermodynamic stability of the solid−liquid and of the solid−solid−liquid equilibria involving the solid solvent.

In a previous work, it was demonstrated that a second liquid phase can emerge only as temperature increases through the ternary monotectic equilibrium $L_{II} \rightleftarrows L_I + S_R + S_S$.[17] First, the temperature of the monotectic equilibrium represents the highest temperature of thermodynamic stability of the solid−solid−liquid equilibrium created by the intersection of the two lower liquidus surfaces of the pure enantiomers. Second, the same temperature is also the lowest temperature of thermodynamic stability of six multiphase equilibria, namely the two solid−liquid equilibria and the solid−solid−liquid equilibrium stemming from the two upper liquidus surfaces of the pure enantiomers, as well as the liquid−liquid equilibrium and the two solid−liquid−liquid equilibria, where the solid is one of the two enantiomers.

The highest temperature of thermodynamic stability of the two solid−liquid equilibria associated with the lower liquidus surfaces and the highest temperature of the two solid−liquid−liquid equilibria are the temperatures of the binary monotectic equilibria $L_{II} \rightleftarrows L_I + S_R$ and $L_{II} \rightleftarrows L_I + S_S$, which are equal as a result of the symmetry of chiral compounds. The eutectic temperature $T_{eut,R-S}$ corresponds to the highest temperature of thermodynamic stability of the solid−solid−liquid equilibrium created by the intersection of the two upper liquidus surfaces of the two enantiomers, while the highest temperature for the solid−liquid equilibria associated with the same liquidus surfaces corresponds to the melting point of the pure enantiomer $T_{m,R}$. Finally, the highest temperature of thermodynamic stability of the liquid−liquid equilibria corresponds to the upper consolution temperature. As a discussion on possible shapes of the liquid−liquid equilibrium surface is beyond the scope of this work, we assume the surface to have either one maximum along the symmetry plane of the ternary phase diagram or two maxima on the lateral planes of the ternary phase diagram.

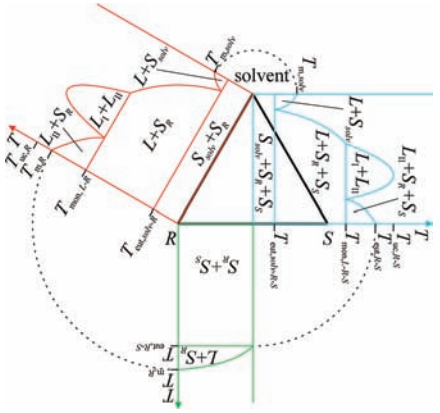

Figure 5. Eutectic, monotectic, melting and upper consolution temperatures defining the topological evolution of the phase diagram of ternary systems forming conglomerates and exhibiting thermodynamically stable oiling out. The three polythermal cuts are turned down. The red one includes the *R*-enantiomer and the solvent; the blue one includes the racemic solid mixture and the solvent; the green phase diagram corresponds to a part of the binary phase diagram of the two enantiomers and is added only for the better understanding of the figure, as all the information it carries is contained in the first two polythermal cuts.

The two binary monotectic equilibria $L_{II} \rightleftarrows L_I + S_R$ and $L_{II} \rightleftarrows L_I + S_S$ are both located on the polythermal cuts referring to the binary systems solvent/pure enantiomer, and as they are identical, the analysis of only one of them suffices. The two liquid phases of the ternary monotectic equilibrium $L_{II} \rightleftarrows L_I + S_R + S_S$ are both racemic[17] and are thus located on the polythermal cut corresponding to the symmetry plane of the ternary phase diagram. Having forced the liquid−liquid equilibrium surface to have its maximum either along the symmetry plane or along the lateral planes of the ternary phase diagram, all relevant states for the determination of the range of thermodynamic stability of all multiphase equilibria are found on two polythermal cuts, one referring to the binary system pure enantiomer/solvent, the other representing the symmetry line of the ternary phase diagram.

The two polythermal cuts are schematically represented in Figure 5. As the liquid−liquid equilibrium covers the whole range of enantiomeric compositions, both polythermal cuts exhibit a eutectic and a monotectic equilibrium. The upper boundaries of the liquid−liquid phase regions are denoted by the upper consolution temperatures $T_{uc,R-S}$ and $T_{uc,R}$.

2.2.3. Generic Phase Diagrams. In order to derive the number of generic phase diagrams, the relative position of the two eutectic equilibria, of the two monotectic equilibria, of the three melting points, and of the two upper consolution temperatures along the temperature axis has to be considered. The conglomerate-forming behavior of the two enantiomers and the constraints applicable to equilibria created by the liquidus surface of the solvent and its intersections with the lower liquidus surfaces of the two enantiomers remain unaltered, therefore the conditions (1), (3), (5) and (6) of Table 1 can be applied also to systems exhibiting oiling out. As liquid−liquid equilibria affect only the solid−liquid equilibria involving the enantiopure solids, the temperature of the ternary monotectic equilibrium $L_{II} \rightleftarrows L_I + S_R + S_S$, $T_{mon,L-R-S}$ has to be larger than the temperature of the ternary eutectic equilibrium $T_{eut,solv-R-S}$. The same applies also

Table 3. Constraints for Monotectic, Eutectic, Melting and Upper Consolution Temperatures Applicable to Conglomerate-Forming Systems Exhibiting Thermodynamically Stable Oiling Out

(1)	$T_{m,R} > T_{eut,R-S}$
(2)	$T_{m,solv} > T_{eut,solv-R-S}$
(3)	$T_{m,solv} > T_{eut,solv-R}$
(4)	$T_{eut,solv-R} > T_{eut,solv-R-S}$
(5)	$T_{mon,L-R-S} > T_{eut,solv-R-S}$
(6)	$T_{mon,L-R} > T_{eut,solv-R}$
(7)	$T_{mon,L-R} > T_{mon,L-R-S}$
(8)	$T_{uc,R-S} > T_{mon,L-R-S}$
(9)	$T_{uc,R} > T_{mon,L-R}$
(10)	$T_{eut,R-S} > T_{mon,L-R-S}$
(11)	$T_{m,R} > T_{mon,L-R}$

for the other polythermal cut, where the temperature of the binary monotectic equilibrium $L_{II} \rightleftarrows L_I + S_R$, $T_{mon,L-R}$, has to be larger than $T_{eut,solv-R}$. Given that the onset of oiling out occurs at the ternary monotectic equilibrium, $T_{mon,L-R-S}$ has to be lower than $T_{mon,L-R}$. Finally, the ternary and the binary monotectic equilibria stemming from the occurrence of oiling out require the upper consolution temperatures $T_{uc,R-S}$ and $T_{uc,R}$ to be larger than $T_{mon,L-R-S}$ and $T_{mon,L-R}$, respectively. The same applies to the eutectic temperature $T_{eut,R-S}$ and to the melting point of the pure enantiomer $T_{m,R}$, which have to be larger than $T_{mon,L-R-S}$ and $T_{mon,L-R}$, respectively. The complete set of constraints is summarized in Table 3.

Permutation of the nine temperatures in compliance with the above-mentioned constraints yields 406 possible ternary phase diagrams, i.e., a very large number. The purpose of this work is to develop generic design strategies for chiral resolution, hence it is essential to obtain exhaustive information on solid−liquid phase equilibria involving the enantiopure solids. In this regard, the two upper consolution temperatures $T_{uc,R-S}$ and $T_{uc,R}$ as well as the melting point of the solvent $T_{m,solv}$ are irrelevant, as these temperatures do not represent any boundary for the temperature ranges of thermodynamic stability of the multiphase equilibria involving the enantiopure solids. As a consequence, the 406 generic phase diagrams can be grouped in five main classes that do not account for these three temperatures. The order of the monotectic, the eutectic and the melting temperatures of these five classes are shown in Table 4. The sequence of the six temperatures is not sufficient to unambiguously define the evolution of the ternary phase diagram, but it provides unambiguous information about the temperature range of thermodynamic stability of the solid−liquid equilibria involving enantiopure solids.

2.2.4. Construction of Qualitative Ternary Phase Diagram from Eutectic, Monotectic, Melting and Upper Consolution Temperatures. The construction of the ternary phase diagram of a system exhibiting oiling out is exemplarily demonstrated by considering a ternary phase diagram of type I, whereby it is assumed that $T_{eut,solv-R} < T_{m,solv} < T_{mon,L-R-S}$ and that both upper consolution temperatures are larger than the melting temperature of the pure enantiomer. A selection of isothermal ternary phase diagrams at increasing temperatures, in this case drawn only qualitatively, is shown in Figure 6. The first liquid phase L emerging from a three-phase solid−solid−solid system at $T_{eut,solv-R-S}$ leads to three solid−liquid and three solid−solid−liquid equilibria slightly above $T_{eut,solv-R-S}$ (Figure 6a).

Table 4. Main Groups of Conglomerate-Forming Systems Exhibiting Thermodynamically Stable Oiling Out Categorized by the Sequence of Monotectic, Eutectic and Melting Temperatures[a]

type I			$T_{eut,R-S}$	$T_{mon,L-R}$	
type II		$T_{eut,solv-R}$	$T_{mon,L-R-S}$	$T_{mon,L-R}$	$T_{eut,R-S}$	
type III	$T_{eut,solv-R-S}$		$T_{eut,R-S}$	$T_{eut,solv-R}$	$T_{mon,L-R}$	$T_{m,R}$
type IV		$T_{mon,L-R-S}$		$T_{mon,L-R}$	$T_{eut,R-S}$	
type V			$T_{eut,solv-R}$	$T_{eut,R-S}$	$T_{mon,L-R}$	

[a] The temperature increases from left to right. Due to their elevated number, the generic phase diagrams have been distributed into five main groups that do not account for the position of three key events $T_{m,solv}$, $T_{uc,R-S}$ and $T_{uc,R}$, which have no impact on the solid-liquid equilibria involving the enantiopure solids and consequently on process design.

At the temperature of the binary eutectic $T_{eut,solv-R}$, the single liquid phase region will reach the sides of the triangle, thus leading to the disappearance of the two solid−solid−liquid phase regions $L + S_{solv} + S_R$ and $L + S_{solv} + S_S$. Increasing the temperature from below (Figure 6b) to above $T_{m,solv}$ (Figure 6c) will lead to the disappearance of the phase region $L + S_{solv}$. At $T_{mon,L-R-S}$, a new liquid phase L_{II} will emerge within the $L + S_R + S_S$ phase region (Figure 6d). The phase regions of the six new phase equilibria that arise from the emergence of L_{II} are shown in Figure 6e. Increasing the temperature, the phase region L_{II} will increase in size and reach the base of the triangle at $T_{eut,R-S}$ (Figure 6f). Passing through an intermediate situation shown in Figure 6g, at $T_{mon,L-R}$, the liquid−liquid phase equilibrium becomes thermodynamically stable for the entire range of enantiomeric excesses, thus leading to the concomitant disappearance of the solid−liquid phase regions $L_I + S_R$ and $L_I + S_S$ and of the solid−liquid−liquid phase regions $L_I + L_{II} + S_R$ and $L_I + L_{II} + S_S$ (Figure 6h). Above this temperature, the liquid−liquid phase region $L_I + L_{II}$ separates the two single phase regions L_I and L_{II}. The two remaining solid−liquid phase regions $L_{II} + S_R$ and $L_{II} + S_S$ are confined to the vicinity of the vertices of the pure enantiomers (Figure 6i) and will disappear at their melting temperature (Figure 6j).

Independent of the type of system, the ternary eutectic equilibrium $L \rightleftarrows S_{solv} + S_R + S_S$ yields a ternary phase diagram with the same number of phase equilibria as the phase diagram shown in Figure 6a. For systems of type I and II, oiling out occurs at temperatures above the binary eutectic temperature $T_{eut,solv-R}$, i.e the two phase regions $L + S_R + S_{solv}$ and $L + S_S + S_{solv}$ are not present at $T_{mon,L-R-S}$. Regarding systems of type III to V, the second liquid phase emerges within the three-phase region of the diagram shown in Figure 6a. Hence, immediately above $T_{mon,L-R-S}$, the isothermal ternary phase diagram will feature all possible multiphase equilibria. In all types of systems, all multiphase equilibria that are thermodynamically stable immediately above $T_{mon,L-R-S}$ will disappear with increasing temperature according to the sequence of the eutectic, the monotectic, the melting and the upper consolution temperatures of the ternary system.

3. CRYSTALLIZATION PROCESS DESIGN

In this and the next section we aim at using the phase diagram demonstrated above to design optimal crystallization processes for the formation of crystals of a single enantiomer, i.e., the target enantiomer.

Upstream of crystallization we assume that there is a process step that yields a partially enriched solution with an enantiomeric

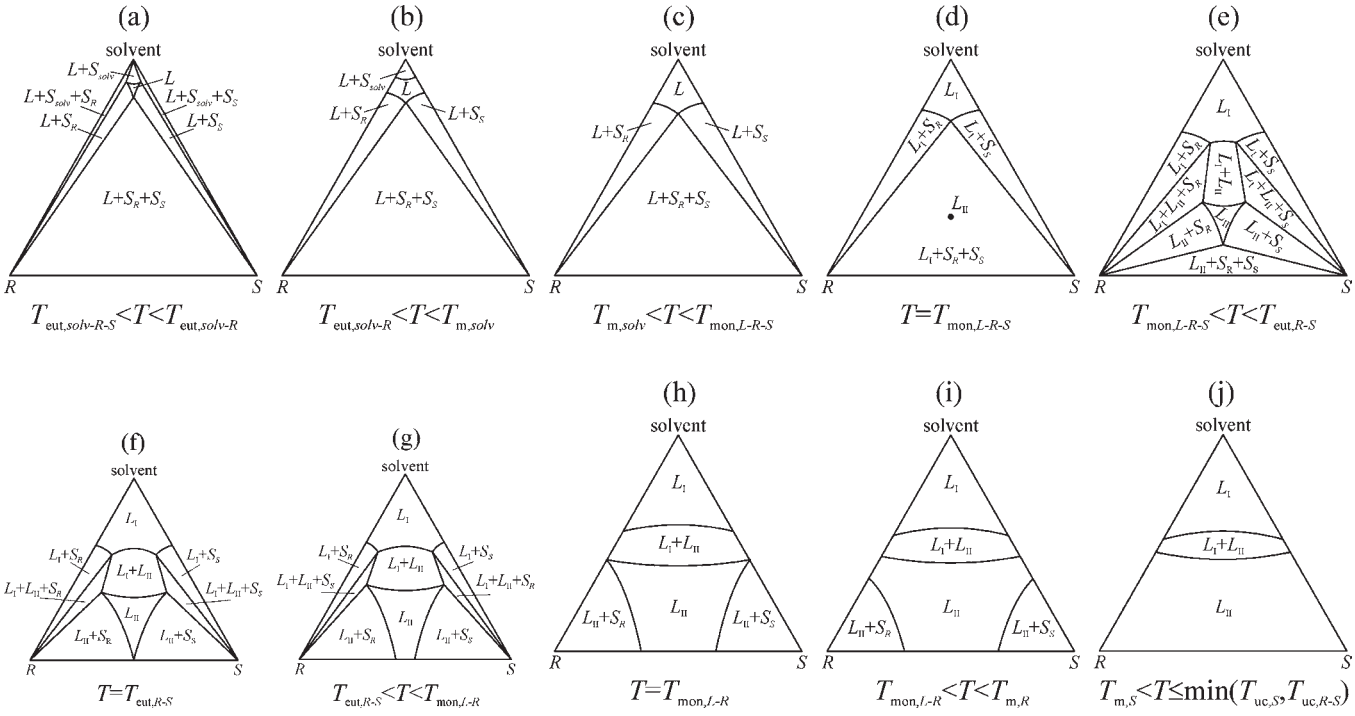

Figure 6. Schematic evolution of the phase diagram of an ideal conglomerate-forming system exhibiting oiling out of type I. The conditions $T_{eut,solv-R} < T_{m,solv} < T_{mon,L-R-S}$ and $T_{uc,R-S}, T_{uc,R} > T_{m,R}$ unambiguously define the evolution of the ternary phase diagram in the temperature range where solid−liquid equilibria are thermodynamically stable.

excess ee_0. Several cases are possible: $ee_0 = 0\%$ if the upstream step is for instance symmetric synthesis; $ee_0 = 100\%$ if there is an infinitely selective upstream step (e.g., highly selective preparative chromatography); ee_0 between 0% and 100% if crystallization is preceded by (partially) enantioselective synthesis or (partial) deracemization, e.g., by chiral chromatography.

The solute concentration is adjusted by addition or removal of solvent so as the solution can be assumed to be a saturated liquid at the initial temperature for crystallization, $T_{initial}$. Cooling down the solution to the final process temperature, T_{final}, a supersaturation is created that is depleted by the formation and growth of new crystals. The design of the crystallization process consists in the choice of an appropriate pair of $T_{initial}$ and T_{final} that allows exploiting the solid−liquid equilibria involving the enantiopure crystals with the aim of selectively crystallizing the target enantiomer, i.e., the one in excess in the feed solution.

Figure 7a and b shows the isothermal ternary phase diagrams at the operating temperatures, i.e., at $T_{initial}$ and T_{final}, of two crystallization processes starting from the same initial temperature and initial enantiomeric excess but ending at different final temperatures.

The state at $T_{initial}$ is described by a single point, i.e., the operating point (blue point in each figure), as the crystallization process is started from a saturated solution. The operating point is at the intersection of the solubility curve at $T_{initial}$ with the straight line at constant enantiomeric excess ee_0, which defines the set of operating points that can be obtained through addition or removal of solvent from the feed solution.

If a final temperature is chosen so that the operating point lies within the solid−liquid-phase region (Figure 7a), only crystals of the target enantiomer will precipitate and grow until equilibrium is reached. The state at T_{final} is represented by two points corresponding to the solid and the liquid phase at equilibrium (magenta points); the solid phase is on the vertex corresponding to the pure target enantiomer. The path the liquid phase follows during the removal of the target enantiomer is defined by the operating line, i.e., a straight line that connects the vertex corresponding to the pure target enantiomer. The intersection of the operating line with the solubility curve at T_{final} defines the final composition of the liquid phase.

If a final temperature is chosen so that the operating point lies within the solid−solid−liquid phase region, besides the target enantiomer also the counter-enantiomer precipitates and grows (Figure 7b). The state at T_{final} is then represented by three points associated with the two solid phases and the liquid phase (magenta points). The solid phases lie on the vertices corresponding to the pure enantiomers. The liquid phase is of racemic composition and, as both enantiomers crystallize, does not belong to the operating line.

The crystallization process shown in Figure 7b is not suitable for chiral resolution as crystals of the counter-enantiomer are formed. The knowledge of the ternary phase diagram is essential for the design of crystallization processes that are not only suitable for chiral resolution but also optimal in the sense defined in the next section.

4. FEASIBLE AND OPTIMAL DESIGN: CRITERIA AND OPERATING DIAGRAMS

4.1. Conglomerate-Forming Systems. *4.1.1. Determination of Operating Points for Crystallization.* Crystallization processes for chiral resolution are carried out at temperatures where solid−liquid equilibria involving the enantiopure crystals of the target enantiomer are thermodynamically stable. The liquid phases involved in these equilibria lie on the liquidus surface of the target enantiomer, and as crystallization processes start from a

dx.doi.org/10.1021/op200191d |Org. Process Res. Dev. 2012, 16, 294–310

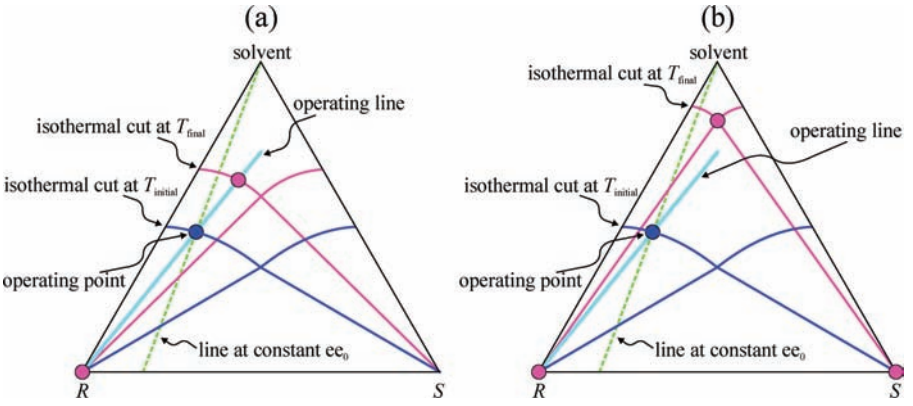

Figure 7. Isothermal ternary phase diagrams at $T_{initial}$ and T_{final} for two crystallization processes starting from the same initial temperature and initial enantiomeric excess but ending at two different final temperatures. The phases that are at equilibrium are denoted by circles. (a) At T_{final}, the operating point lies within the solid−liquid phase region involving the crystals of the target enantiomer. (b) At T_{final}, the operating point lies within the solid−solid−liquid equilibrium involving the crystals of the two enantiomers.

saturated solution, also the operating points lie on the same liquidus surface at $T_{initial}$. Hence, the portion of the liquidus surface of the target enantiomer that is thermodynamically stable defines the set of operating points that are suitable for crystallization.

Independent of the type of system, the liquidus surface of the target enantiomer is delimited by its intersection with the liquidus surfaces of the counter-enantiomer and of the solvent. The points of intersection between liquidus surfaces lie on monovariant curves connecting the liquid phases involved in the binary eutectic equilibria on the lateral planes of the ternary prism with the liquid phase involved in the ternary eutectic equilibrium located on the symmetry plane of the prism. Having three thermodynamically stable liquidus surfaces in any conglomerate-forming system, the ternary phase diagram always exhibits three monovariant curves, which meet at the point corresponding to the liquid phase of the ternary eutectic equilibrium.[24]

The liquidus projection, where the projections of the monovariant curves onto the base of the ternary prism are plotted, allows determining the operating points that are feasible for chiral resolution by crystallization. The pink region in the liquidus projection shown in Figure 8 shows the set of possible operating points in the case where the *R*-enantiomer is the target enantiomer.

4.1.2. Determination of Operating Temperatures for Crystallization. The temperatures that are required to saturate ternary mixtures of different composition decrease with decreasing ee_0 and solute concentration. Independent of the type of system, $T_{m,R}$, i.e., the temperature corresponding to the point on the liquidus surface with the highest solute concentration and enantiomeric enrichment, is larger than both $T_{eut,solv-R}$, corresponding to the point with the same enantiomeric enrichment but with the lowest solute concentration, and $T_{eut,R-S}$, corresponding to the point with the same solute concentration but of racemic composition. Furthermore, $T_{eut,solv-R}$ and $T_{eut,R-S}$ are larger than $T_{eut,solv-R-S}$, i.e., the temperature corresponding to the point of racemic composition with the lowest solute concentration.

The highest $T_{initial}$ value for a set of operating points with constant ee_0 required liquefying a binary mixture of the two enantiomers, decreases from $T_{m,R}$ to $T_{eut,R-S}$ when dropping ee_0 from 100% to 0%. Its lowest $T_{initial}$ value, which is required to liquefy a ternary mixture corresponding to the most diluted

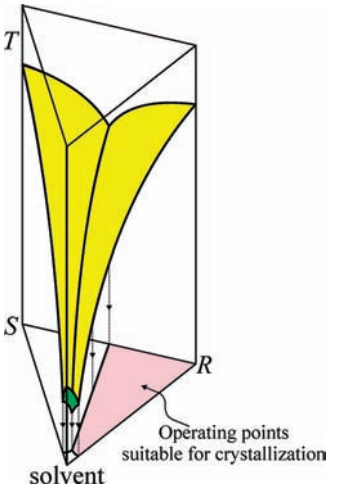

Figure 8. Schematical liquidus projection of the ternary phase diagram of a simple conglomerate-forming system. The pink region, delimited by monovariant eutectic curves, contains operating points that are suitable for the crystallization of the *R*-enantiomer.

operating point, also decreases when decreasing ee_0 from 100% to 0%: it goes from $T_{eut,solv-R}$ to $T_{eut,solv-R-S}$.

For each operating point, the highest final temperature is its saturation temperature, i.e., $T_{initial}$, whereas the lowest final temperature is always the temperature of the ternary eutectic equilibrium $T_{eut,solv-R-S}$, because below this temperature only solid phases can be obtained.

4.1.3. Determination of Feasible Operating Temperatures for Chiral Resolution. For any operating point that is suitable for crystallization, only one temperature out of the set of possible final temperatures allows crystallizing the target enantiomer selectively and maximizing the yield, i.e., the ratio between the mass of final crystals of the target enantiomer and the mass of target enantiomer in the feed solution. The yield *Y* can be calculated from the concentration of the target enantiomer in the liquid phase at the initial and at the final process temperature as follows:

$$Y = \frac{c_{R,\,initial} - c_{R,\,final}}{c_{R,\,initial}} \qquad (2)$$

dx.doi.org/10.1021/op200191d |*Org. Process Res. Dev.* 2012, 16, 294–310

The enantiomeric excess ee (in percentage) can be calculated using the following equation:

$$ee = 100 \cdot \frac{c_R - c_S}{c_R + c_S} \quad (3)$$

where c_R and c_S are the concentrations of the *R*- and the *S*-enantiomer in the liquid phase, respectively. The concentrations in eqs 2 and 3 are expressed in mass of solute per mass of solvent.

Considering that in chiral resolution processes the concentration of the counter-enantiomer remains constant throughout the process, i.e., $c_{S,initial} = c_{S,final}$, the yield can be expressed as a function of the initial and the final enantiomeric excess only:[25]

$$Y = 1 - \frac{(1 - ee_0)(1 + ee_{final})}{(1 + ee_0)(1 - ee_{final})} \quad (4)$$

The yield is increased by decreasing ee_{final}, which reaches its minimum when the liquid phase at equilibrium at T_{final} has eutectic composition, i.e., it lies on a monovariant curve. In this case the position of the operating line at T_{final} coincides with the line separating the solid−liquid from the solid−solid−liquid phase region. Intersections between the liquidus surfaces of the two enantiomers yield monovariant eutectic equilibria involving racemic liquid phases, whereas intersections between the liquidus surfaces of one enantiomer and of the solvent yield monovariant eutectic equilibria involving liquid phases varying from racemic to enantiopure composition. For conglomerate-forming systems, the eutectic liquid phase with the lowest enantiomeric excess has racemic composition. Therefore, the operating points whose operating line crosses the monovariant curve at a point of racemic composition, i.e., where $ee_{final} = 0$, allow obtaining the global maximal yield, which corresponds to:[25]

$$Y_{global,max} = \frac{2ee_0}{(1 + ee_0)} \quad (5)$$

The maximal yield of all other operating points decreases from $Y_{global,max}$ to 0 depending on the enantiomeric excess of the eutectic liquid phase at T_{final} and corresponds only to a local maximum. The set of operating points can therefore be divided in two classes depending on the maximal yield possible. Therefore the operating line passing through the liquid phase of the ternary eutectic equilibrium separates the two classes of operating points (Figure 9). Operating points on or below this line (green region in the same figure) allow for chiral resolution processes attaining the global maximal yield.

For a specific operating point, any final temperature between $T_{initial}$ and the optimal final temperature yields an equilibrium involving crystals of the target enantiomer and a liquid phase enantiomeric excess larger than zero. Hence, for these final temperatures chiral resolution is feasible but the yield is not maximal. In the case where final temperatures below the optimal final temperature are chosen, the operating point lies in a three-phase region where crystals of either the counter-enantiomer or the solvent become thermodynamically stable and might crystallize, thus leading to a loss of performance of the chiral resolution process. Thus, for any value of $T_{initial}$, the final temperature that maximizes the yield represents always the lowest final temperature that allows for chiral resolution.

4.1.4. Design Criteria for an Ideal Conglomerate-Forming System of Type I. For the system of type I discussed in Section 2.1.4, Figure 10a and b shows the isothermal ternary phase diagrams at two operating temperatures for two chiral resolutions

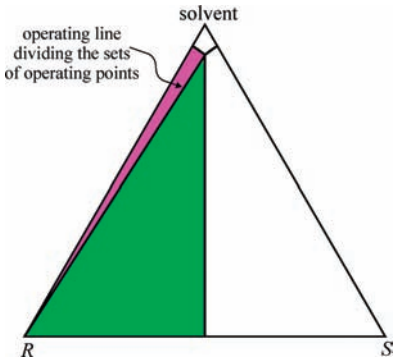

Figure 9. Schematical liquidus projection of simple conglomerate-forming systems. The line separating the two regions corresponds to the operating line that passes through the liquid phase of the ternary eutectic equilibrium. Operating points in the green region including the operating line allow obtaining the global maximal yield, while the ones in the magenta region allow obtaining the local maximal yield.

both starting from a feed solution with $ee_0 = 50\%$ and leading to maximal yield.

The operating point shown in Figure 10a has a higher solute concentration than the one shown in Figure 10b. As crystallization is started from a saturated solution, both operating points lie on the (blue) solubility isotherms at the initial temperature of crystallization. If a clear solution, whose composition corresponds to the operating point of Figure 10a, is cooled down to the temperature represented by the green solubility isotherms, an equilibrium is obtained between crystals of the target enantiomer and a racemic liquid phase (green dot in the same figure), which has the lowest possible enrichment. This operating point therefore allows reaching the global maximal yield. If reported in the liquidus projection of Figure 9, the operating point would lie inside the green region, and its operating line would cross the monovariant curve through racemic liquid phases. For the operating point of Figure 10b, however, no final temperature exists, which allows reaching an equilibrium involving a racemic liquid phase. The eutectic liquid phase (green dot in the same figure), which maximizes the yield, arises from the intersection between the liquidus surfaces of the target enantiomer and of the solvent. The operating point of Figure 10b therefore allows reaching the local maximal yield only. In the liquidus projection of Figure 9, the operating point is part of the magenta region, and its operating line crosses the monovariant curve through non-racemic liquid phases.

The determination of optimal $T_{initial}$ and T_{final} values can be repeated for all operating points at constant ee_0, resulting in a set of pairs of optimal operating temperatures. This set can be split in two subsets, i.e., those operating points reaching the global maximal yield and the others. Plotting the points with optimal operating temperatures as coordinates in the T_{final} versus $T_{initial}$ plane, which will be called the operating plane in the following, two curves are obtained as shown in Figure 10a: the solid line represents operating temperatures yielding the global maximal yield, whereas the yield of points with operating temperatures on the dashed line correspond only to the local maximum. At the lowest initial temperature, the operating point is of eutectic composition. In this case $T_{initial}$ and T_{final} are equal and define a point on the diagonal of the operating plane.

Along the solid line in the operating plane, the yield is constant but the solvent mass fraction increases with decreasing initial and

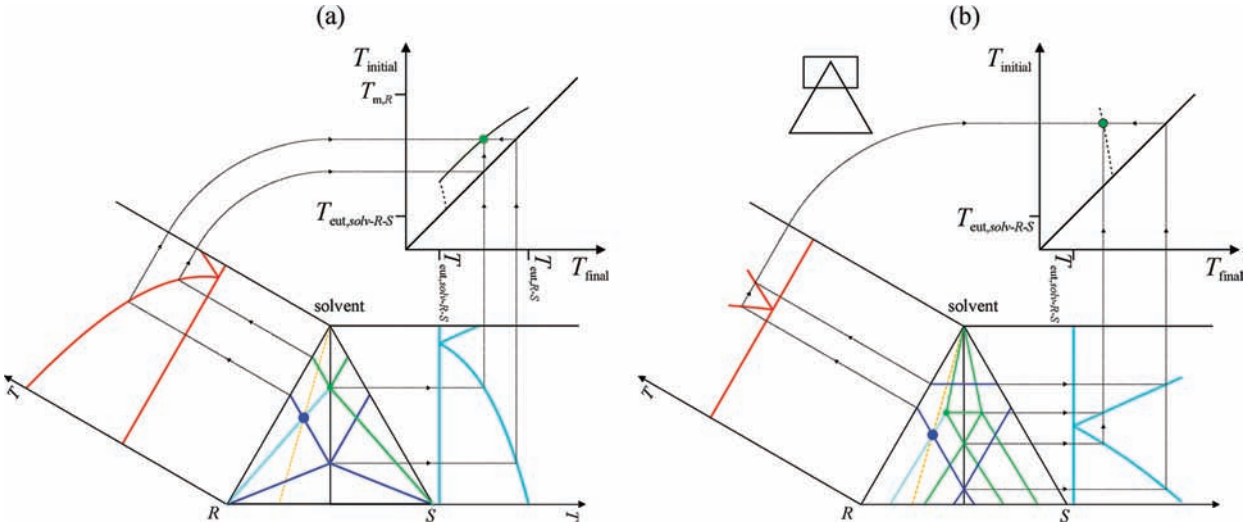

Figure 10. Isothermal ternary phase diagrams at $T_{initial}$ and T_{final} for two chiral resolution processes starting from the same ee_0 value for the ideal conglomerate-forming system of type I presented in Section 2.1.4. (a) Case where the global maximal yield is obtained. (b) Case where only the local maximal yield is obtained. The ternary phase diagram in panel b refers only to the upper part of the complete ternary phase diagram (see insert). The blue lines define the isothermal ternary phase diagram at $T_{initial}$, while the green lines define the one at T_{final}. The circles indicate the composition of the liquid phases at equilibrium at the two operating temperatures. The light-blue lines within the triangle represent the operating lines, and the yellow lines represent the lines at constant ee_0.

final temperatures, as the saturation temperature decreases with increasing solvent mass fraction. Along the dashed line, the yield decreases while the solvent mass fraction increases with decreasing $T_{initial}$. The two monovariant curves in the liquidus projection consisting of the liquid phases that are at equilibrium at the optimal final temperatures meet at the point corresponding to the liquid phase of the ternary eutectic equilibrium. Hence, the two curves in the operating plane containing optimal operating temperatures have a common point at the final temperature corresponding to the ternary eutectic temperature $T_{eut,solv-R-S}$, which is the lowest possible final temperature for crystallization.

The pairs of $T_{initial}$ and T_{final} values for a specific ee_0 span an area in the operating plane where crystallization is feasible. The colored areas in Figure 11 indicate the area spanned by the sets of suitable operating temperatures for an initial enantiomeric excess of 50%. The solid and the dashed lines correspond to the curves of optimal operating temperatures shown in Figure 10a. As T_{final} values above the optimal final temperature lead to solid−liquid equilibria involving crystals of the target enantiomer only, the points within the blue region are also suitable for chiral resolution, but the larger the horizontal distance from the solid and the dashed line, the smaller the yield. On the other hand, final temperatures below the optimal value are unsuitable for chiral resolution. The solid line separates the region suitable for chiral resolution from the unsuitable region where crystals of the counter-enantiomer form (yellow region), while the dashed line separates it from a second unsuitable region where crystals of the solvent form (red region).

The determination of the optimal operating conditions and, consequently, of the different regions in the operating plane can be repeated for all ee_0 values. Figure 9 indicates that the classification of operating points based on the maximal possible yield is independent of ee_0. Considering operating points on the same operating line, i.e., operating points with the same optimal T_{final} value but with different ee_0, the higher ee_0, the higher the solute concentration and hence also the initial temperature.

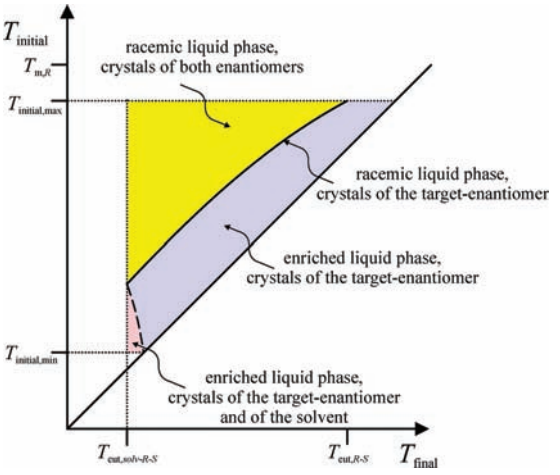

Figure 11. T_{final} versus $T_{initial}$ diagram for the ideal conglomerate-forming system of type I of Section 2.1.4 for an initial enantiomeric excess of 50%. The three colored areas correspond to the area spanned by the sets of T_{final} and $T_{initial}$ that allow for crystallization. The solid line contains pairs of operating temperature that allow obtaining the global maximal yield, whereas the dashed line contains pairs of operating temperatures that allow obtaining the local maximal yield only.

Therefore the optimal operating curves defined by the pairs of operating temperatures giving the global and the local maximal yield shift to higher initial temperatures with increasing ee_0. The two curves of optimal operating temperatures for different ee_0 values are shown in Figure 12. The range of final temperatures that leads to the global maximal yield coincides with the range of thermodynamic stability of the solid−solid−liquid equilibrium involving the two enantiopure crystals, i.e., from $T_{eut,solv-R-S}$ to $T_{eut,R-S}$, and is independent of ee_0. Moreover, for any ee_0 value the two optimal operating curves divide the area of suitable operating conditions for crystallization (colored areas

dx.doi.org/10.1021/op200191d |*Org. Process Res. Dev.* 2012, 16, 294–310

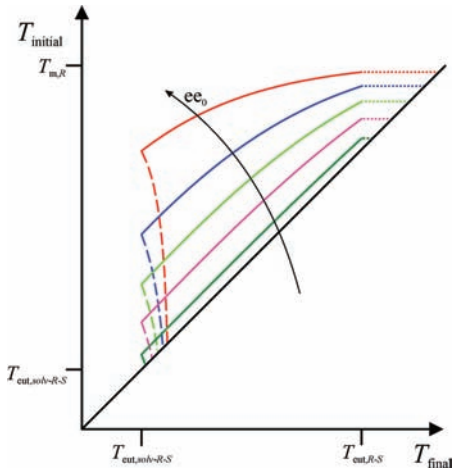

Figure 12. Curves representing pairs of optimal operating temperatures for the ideal conglomerate-forming system of type I presented in Section 2.1.4 for different initial enantiomeric enrichments. The solid lines contain pairs of operating temperatures that allow obtaining the global maximal yield, whereas the dashed lines contain pairs of operating temperatures that allow obtaining the local maximal yield only. For each ee_0, the region delimited by the bisecting line, the solid, the dashed and the dotted lines contain pairs of operating temperatures that are suitable for chiral resolution.

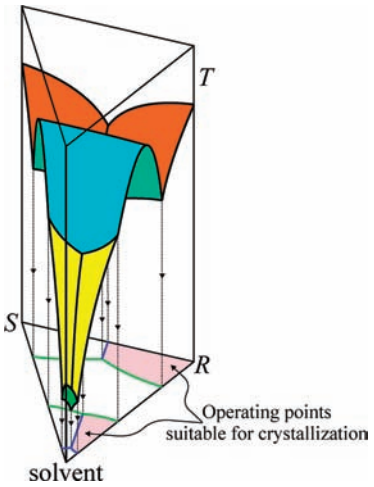

Figure 13. Schematical liquidus projection of a conglomerate-forming system exhibiting oiling out as discussed in Section 2.2. The four blue curves represent monovariant eutectic curves. The four green curves represent monovariant monotectic curves. The pink areas show the set of operating points that are suitable for crystallization.

in Figure 11) in three different regions, namely, one that is suitable for chiral resolution and two that are not.

The operating diagrams for different ee_0 values shown in Figure 12 have to be interpreted as completed by their information about operating regions as shown in Figure 11 for one specific ee_0 value. Thus, Figure 12 provides a complete picture about feasible and optimal conditions for chiral resolution, which are based on the phase diagram.

4.2. Conglomerate-Forming Systems Exhibiting Oiling Out. *4.2.1. Determination of Operating Points for Crystallization.* In the ternary phase diagrams of conglomerate-forming systems exhibiting oiling out (see Section 2.2 and Figure 13), for each enantiomer two liquidus surfaces are present, which are separated from each other by the surface corresponding to the liquid−liquid phase equilibria. As crystallization processes are started from saturated solutions, the portions of the two liquidus surfaces belonging to the target enantiomer that are thermodynamically stable define the set of operating points that are suitable for crystallization. The upper liquidus surface is in all cases delimited by its intersections with the solute-rich part of the liquid−liquid equilibrium surface and by the upper liquidus surface of the counter-enantiomer, while the lower liquidus surface is delimited by its intersection with the solute-lean part of the liquid−liquid equilibrium surface, the liquidus surface of the solvent and the lower liquidus surface of the counter-enantiomer.

The liquidus projection of these systems, schematically represented in Figure 13, contains eight monovariant curves. The four blue curves describe the compositions of the liquid phases involved in monovariant eutectic equilibria, while the four green curves describe the compositions of the two liquid phases involved in monovariant monotectic equilibria. As a result of the lack of enantioselectivity of the solvent, points lying on the monovariant monotectic curves having equal enantiomeric excess are at equilibrium, i.e., they are connected by straight tie-lines that go through the solvent vertex. The three monovariant eutectic curves on the border of the lower liquidus surfaces connect the liquid phases of the two binary eutectic equilibria involving the solvent and the solute-lean liquid phase of the ternary monotectic equilibrium with the liquid phase of the ternary eutectic equilibrium. The four monovariant monotectic curves connect the two liquid phases of the two binary monotectic equilibria with the liquid phases of the ternary monotectic equilibrium. Finally, the monovariant eutectic curve separating the two upper liquidus surfaces connects the liquid phase of the binary eutectic equilibrium with the solute-rich liquid phase of the ternary monotectic equilibrium.

The two pink regions in the liquidus projection shown in Figure 13 represent the operating points that are feasible for crystallization in the case where the *R*-enantiomer is the target enantiomer.

4.2.2. Determination of Operating Temperatures for Crystallization. Also for systems exhibiting oiling out, the temperatures required to saturate ternary mixtures decrease with decreasing initial enantiomeric excess and solute concentration. This can be demonstrated by comparing the temperatures at the four corners of the two liquidus surfaces of the target enantiomer. On the upper liquidus surface, $T_{m,R}$ is larger than both $T_{eut,R-S}$ and $T_{mon,L-R}$, whereas the latter two temperatures are larger than $T_{mon,L-R-S}$. On the lower liquidus surface, $T_{mon,L-R}$ is larger than both $T_{mon,L-R-S}$ and $T_{eut,solv-R}$, which are in turn larger than $T_{eut,solv-R-S}$.

The highest $T_{initial}$ value for a set of operating points at constant initial enantiomeric excess ee_0 decreases from $T_{m,R}$ to $T_{eut,R-S}$ when decreasing ee_0 from 100% to 0%. For any ee_0 value, the most diluted operating point on the upper liquidus surface and the most concentrated operating point on the lower liquidus surface also belong to the surface corresponding to the liquid−liquid equilibria. As the tie-lines describing liquid−liquid equilibria connect liquid phases with the same enantiomeric excess, the two liquid phases are part of the same liquid−liquid equilibrium. Hence, the lowest $T_{initial}$ value for operating points lying on the upper liquidus surface is equal to the highest $T_{initial}$ value for operating points lying on the lower liquidus surface and varies from $T_{mon,L-R}$ at ee_0 = 100% to $T_{mon,L-R-S}$ at ee_0 = 0%. Finally, the lowest $T_{initial}$ value, required to saturate a mixture

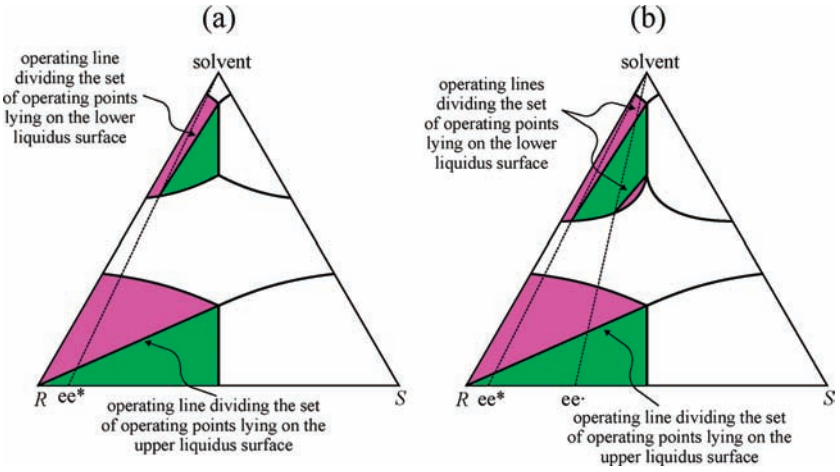

Figure 14. Liquidus projections of the ternary phase diagram of two conglomerate-forming systems exhibiting oiling out as discussed in Section 2.2. (a) No monotectic liquid phase maximizes the yield of any operating point lying on the lower liquidus surface at $T_{initial}$. (b) Monotectic liquid phases maximize the yield for a limited number of operating points lying on the lower liquidus surface at $T_{initial}$. In both figures, operating points in the green regions allow obtaining the global maximal yield, while the ones in the magenta regions allow obtaining the local maximal yield only. ee* is the largest initial enantiomeric excess that allows obtaining the global maximal yield independent of which liquidus surfaces the operating point lies at $T_{initial}$. ee′ is the enantiomeric excess of the monotectic liquid phase with the highest enantiomeric excess that maximizes the yield.

corresponding to the most diluted operating point with a given ee_0, decreases when decreasing ee_0 from 100% to 0%, namely, from $T_{eut,solv-R}$ to $T_{eut,solv-R-S}$.

The set of possible final temperatures for each operating point ranges from its saturation temperature, i.e., $T_{initial}$, to the temperature of the ternary eutectic equilibrium $T_{eut,solv-R-S}$.

4.2.3. Determination of Feasible Operating Temperatures for Chiral Resolution. After determining the set of operating points, the final temperature that maximizes the yield for each of them can be determined. In processes with operating points lying on the upper liquidus surface at $T_{initial}$, the liquid phases at equilibrium at the optimal final temperatures can have either eutectic or monotectic composition. Liquid phases of eutectic composition are racemic, as they arise from intersections between the two upper liquidus surfaces of the pure enantiomers. The liquid phases of monotectic composition vary from racemic to enantiopure composition, as they are at the intersection between the solute-rich part of the liquid−liquid equilibrium surface and the upper liquidus surface of the target enantiomer.

The liquid phases that can be obtained at the optimal final temperatures for operating points lying on the lower liquidus surface at $T_{initial}$ depend on the steepness and on the curvature of the monovariant monotectic curve delimiting the lower liquidus surface. Figure 14a shows the case where no monotectic liquid phase exists that maximizes the yield of any operating point. Thus, the possible liquid phases are of eutectic composition and are racemic if the liquid phases belong to a monovariant eutectic equilibrium involving the two enantiopure crystals, whereas they vary between racemic and enantiopure composition when the liquid phase is part of a monovariant equilibrium involving crystals of the target enantiomer and of the solvent. Figure 14b shows the case where for a limited number of operating points the yield is maximized when an equilibrium involving a monotectic liquid phase is obtained. In this case the liquid phases at the optimal final temperatures can be either eutectic or monotectic, whereby the monotectic liquid phases vary from ee′ to 0% (ee′ is the enantiomeric excess of the intersection point between the monotectic curve and the operating line passing through the solute-lean liquid phase of the ternary monotectic equilibrium).

Hence, operating points on both the upper and the lower liquidus surface exist that allow obtaining the global maximal yield. From this it follows that the set of operating points of each liquidus surface can be divided into two classes based on the maximal yield possible, namely, whether it corresponds to the global maximum (green regions in Figure 14a and b including the lines delimiting them) or to the local maximum (magenta regions).

The operating line passing through the solute-rich liquid phase of the ternary monotectic equilibrium divides the set of operating points lying on the upper liquidus surface at any $T_{initial}$-level in two parts. In the liquidus projection shown in Figure 14a, the operating line passing through the liquid phase of the ternary eutectic equilibrium divides the set of operating points lying on the lower liquidus surface at any $T_{initial}$ value also in two parts. In the liquidus projection of Figure 14b, the two operating lines passing through the liquid phase of the ternary eutectic equilibrium and through the solute-lean liquid phase of the ternary monotectic equilibrium, respectively, divide the two classes of operating points lying on the lower liquidus surface.

For initial enantiomeric excesses lower than ee*, the global maximal yield can be reached independently of which liquidus surface the operating point lies at $T_{initial}$, whereas for initial enantiomeric excesses larger than ee*, the global maximal yield can only be reached for operating points lying on the upper liquidus surface.

Independent of the composition of the operating points, a final temperature in the range between $T_{initial}$ and the optimal final temperature allows for chiral resolution, since in this case an equilibrium is reached involving enantiopure crystals of the target enantiomer and a liquid phase with an enantiomeric excess larger than the corresponding eutectic or monotectic composition. At any final temperature below the optimal final temperature, the operating points lie in a three-phase equilibrium where either a second liquid phase or crystals of either the counter-enantiomer or of the solvent become thermodynamically stable and might

dx.doi.org/10.1021/op200191d |*Org. Process Res. Dev.* 2012, 16, 294–310

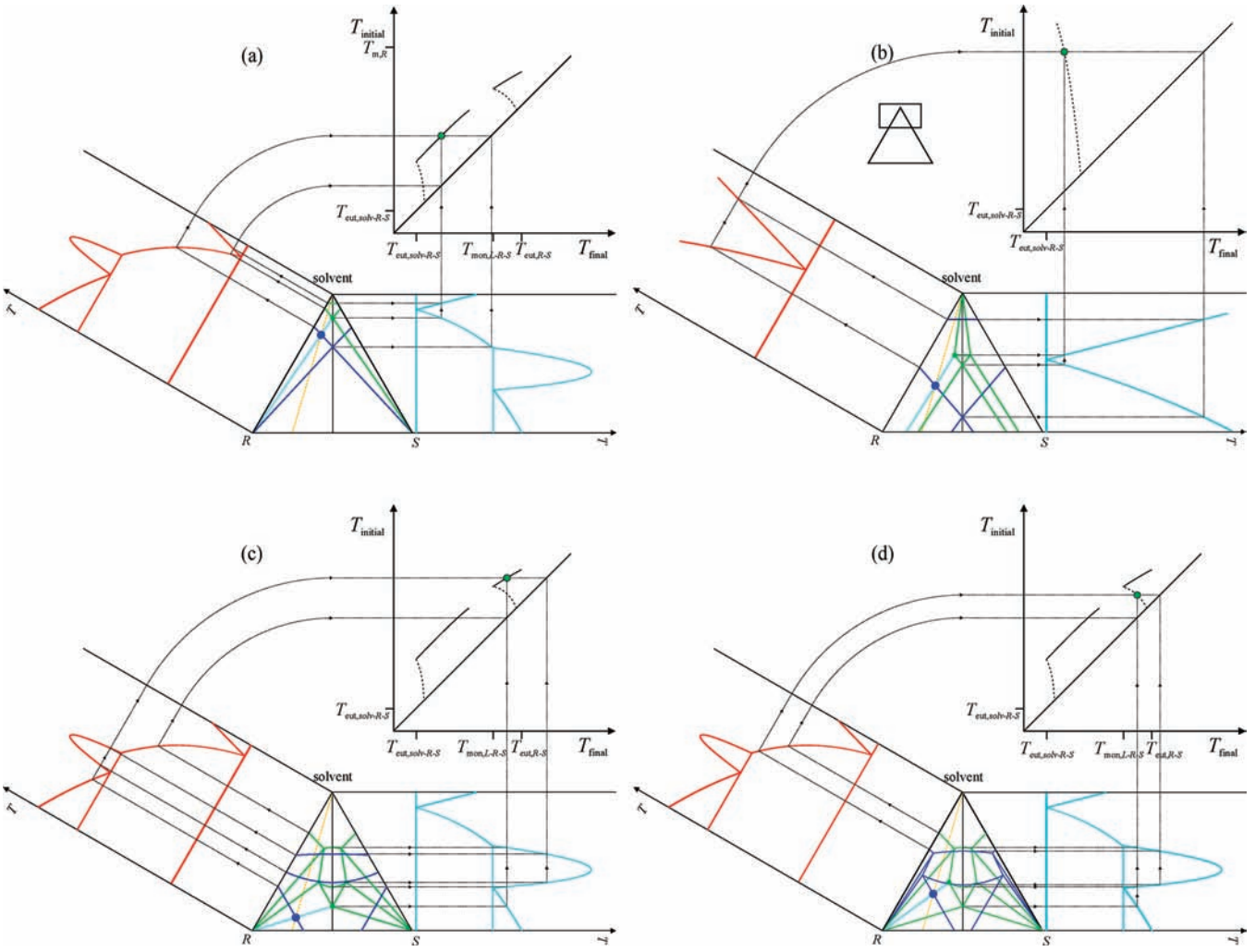

Figure 15. Isothermal ternary phase diagrams at $T_{initial}$ (blue lines) and T_{final} (green lines) for four chiral resolution processes at constant ee_0 for a hypothetical conglomerate-forming system exhibiting oiling out of type I, where $T_{eut,solv-R} < T_{m,solv} < T_{mon,L-R-S}$ and $T_{uc,R-S}, T_{uc,R} > T_{m,R}$. ee_0 is the same for all operating points and is larger than ee*. Furthermore, no monotectic liquid phase is obtained at any optimal final temperature of operating points lying on the lower liquidus surface. The operating points in cases (a) and (b) lie on the lower liquidus surface at $T_{initial}$, while in cases (c) and (d) they lie on the upper liquidus surface at $T_{initial}$. In cases (a) and (c), the global maximal yield is reached. The circles indicate the composition of the liquid phase at equilibrium at the two operating temperatures. The ternary phase diagram in panel b refers only to the upper part of the complete ternary phase diagram (see insert). The light-blue lines within the triangle represent the operating lines, and the yellow lines represent the lines at constant ee_0.

crystallize, thus leading to a loss of performance of the chiral resolution process. As in the case of simple conglomerate-forming systems, for all operating points the lowest final temperature possible for chiral resolution corresponds to their optimal final temperature.

4.2.4. Design Criteria for a Conglomerate-Forming System Exhibiting Oiling out of Type I. We are considering a conglomerate-forming system of type I, more specifically one whose liquidus projection corresponds to that shown in Figure 14a. Such a system is hypothetical but verisimilar since an example of a real system exhibiting such behavior has been documented earlier.[17] Let us consider operating points, whose enantiomeric excesses are equal and smaller than ee*. According to Figure 14a, the set of possible operating points can be split in four different subsets, based on which liquidus surface the operating point at $T_{initial}$ lies and based on whether it allows reaching the global maximal yield or not. In Figure 15a to d one operating point out of each subset is considered. The two operating points in Figure 15a and b lie on the lower liquidus surface at $T_{initial}$ (right yellow liquidus surface in Figure 13). The operating point in Figure 15a allows reaching the global maximal yield and is therefore an element of the upper green surface in the liquidus projection shown in Figure 14a, while the one in Figure 15b allows reaching the local maximal yield only and thus belongs to the upper magenta surface in Figure 14a. The two operating points shown in Figure 15c and d lie on the upper liquidus surfaces at $T_{initial}$ (right orange surface in Figure 13). Only the operating point in Figure 15c allows reaching the global maximal yield and is element of the lower green surface in Figure 14a, while the one in Figure 15c belongs to the lower magenta region of the same figure. The optimal pairs of $T_{initial}$ and T_{final} values for each operating point at constant ee_0 can be determined, yielding four subsets of pairs of optimal operating temperatures.

In the operating plane, the four subsets of pairs of T_{final} and $T_{initial}$ values maximizing the yield define points belonging to four curves. The two solid curves represent the pairs of operating

dx.doi.org/10.1021/op200191d |*Org. Process Res. Dev.* 2012, 16, 294–310

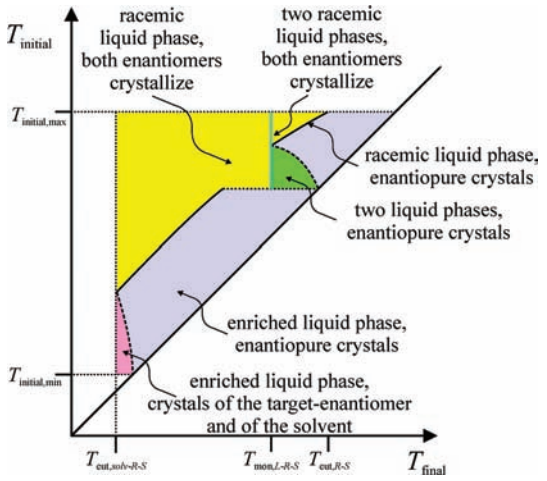

Figure 16. T_{final} versus $T_{initial}$ plane for a hypothetical conglomerate-forming system exhibiting oiling out of type I. The liquidus projection qualitatively corresponds to the one shown in Figure 14a and ee_0 is smaller than ee*, thus the diagram exhibits four curves containing optimal operating temperatures. The solid lines pass through pairs of operating temperatures giving the global maximal yield, the dashed line contains operating temperatures that allow obtaining the local maximal yield only. The five colored areas correspond to the area spanned by the sets of operating temperatures that allow for crystallization.

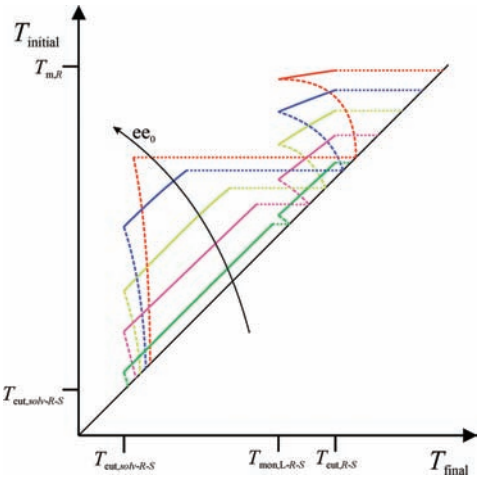

Figure 17. Curves representing pairs of optimal temperatures for a hypothetical conglomerate-forming system exhibiting oiling out of type I for different initial enantiomeric excesses. No equilibria involving a monotectic liquid phase exist that maximize the yield of operating points lying on the lower liquidus surface. The solid lines represent pairs of operating temperature that allow obtaining the global maximal yield. The dashed lines contains pairs of operating temperatures that allow obtaining the local maximal yield. For each ee_0, the two regions delimited by the bisecting line, the solid, the dashed and the dotted lines contain operating temperatures that are suitable for chiral resolution.

temperatures giving the global maximal yield, whereas the two dashed curves represent pairs of operating temperatures leading to the local maximal yield. The most diluted operating points on the upper and on the lower liquidus surfaces have monotectic and eutectic composition, respectively. Hence, the optimal temperatures of these two operating points are equal and lie on the diagonal of the operating plane.

As the two monovariant eutectic curves delimiting the lower liquidus surface meet at the point corresponding to the liquid phase of the ternary eutectic equilibrium, the two curves of operating points lying on the lower liquidus surface at $T_{initial}$ have one common point at $T_{eut,solv-R-S}$. The other two curves of optimal operating temperatures have a common point at $T_{mon,L-R-S}$, as the monovariant monotectic and eutectic curves delimiting the upper liquidus surface meet at the point corresponding to the solute-rich liquid phase of the ternary monotectic equilibrium. The temperatures $T_{eut,solv-R-S}$ and $T_{mon,L-R-S}$ correspond to the lowest optimal final temperatures for operating points lying on the lower and on the upper liquidus surface, respectively.

The colored domains in Figure 16 show the area spanned by pairs of T_{final} and $T_{initial}$ values that allow for crystallization for a specific ee_0. The solid and the dotted lines represent the pairs of operating temperatures maximizing the yield already shown in Figure 15. As any final temperature equal or above the optimal value allows selectively crystallizing the target enantiomer, the two blue regions including the lines delimiting them contain operating temperatures that are suitable for chiral resolution. Pairs of operating temperatures within the other three regions are unsuitable for chiral resolution as a third undesired phase becomes thermodynamically stable and might crystallize. If operating temperatures within the green region are chosen, the crystals of the target enantiomer are at equilibrium with two liquid phases at T_{final}. Operating temperatures within the yellow and the red region yield solid−solid−liquid equilibria involving crystals of the counter-enantiomer and of the solvent, respectively, as the second solid phase.

The two yellow regions in Figure 16 are separated by the blue vertical line at the final temperature equal to the ternary monotectic temperature, $T_{mon,L-R-S}$. At any final temperatures above $T_{mon,L-R-S}$, the liquid phase, which is at equilibrium with crystals of the two enantiomers, is racemic and is part of the two upper liquidus surfaces of the two enantiomers. On the blue vertical line, a ternary monotectic equilibrium consisting of two racemic liquid phases and crystals of the two enantiomers is obtained (Figure 6d). At final temperatures below $T_{mon,L-R-S}$, the racemic liquid phase, which is at equilibrium with crystals of the two enantiomers, is part of the two lower liquidus surfaces of the two enantiomers. The green region in Figure 16 is delimited by the blue vertical line representing the ternary monotectic equilibrium. Any operating point leading to a liquid−liquid-solid equilibrium above $T_{mon,L-R-S}$ will yield a liquid−solid−solid equilibrium involving crystals of the two enantiomers at temperatures below $T_{mon,L-R-S}$. The transition from a liquid−liquid−solid equilibrium to a liquid−solid−solid equilibrium induced by lowering the temperature occurs through a ternary monotectic reaction.

The determination of the five regions in the operating plane can be repeated for all ee_0 values. Figure 17 shows the curves bounding these regions for different ee_0 values. Analogous to simple conglomerate-forming systems, the curves corresponding to optimal temperatures are shifted to higher initial temperatures when increasing the initial enantiomeric excess. For all ee_0, two regions that are suitable for chiral resolution are obtained.

At least one operating point for each ee_0 value lying on the upper liquidus surface at $T_{initial}$ allows obtaining the global maximal yield. Hence, the curve containing operating temperatures giving the global maximal yield is present for all ee_0 values. On the other hand, for operating points on the lower liquidus

dx.doi.org/10.1021/op200191d |*Org. Process Res. Dev.* 2012, 16, 294–310

surface the global maximal yield can only be reached for operating points with an initial enantiomeric excess below ee*. The highest initial enantiomeric excess considered in Figure 17 is larger than ee*, and therefore no curve of operating temperatures giving the global maximal yield exists for an operating point lying on the lower liquidus surface at $T_{initial}$.

Once again Figure 17 provides a complete characterization of feasible and optimal operating temperatures to achieve chiral resolution through crystallization, whatever the initial enantiomeric excess.

5. DISCUSSION AND CONCLUSIONS

5.1. Process Design and Generalization. The outcome of the process design for the two systems discussed in Section 4.1.4 and Section 4.2.4 can be generalized to all types of conglomerate-forming systems.

For simple conglomerate-forming systems, the possible operating points lie on the single liquidus surface associated with the target enantiomer, hence, they belong to a single connected region in the liquidus projection (pink region in Figure 8). Independent of the type of system, the region is delimited by a monovariant eutectic curve featuring racemic liquid phases, which arises from the intersection among the two liquidus surfaces associated with the two enantiomers. The operating points, whose operating line crosses this curve, lead to the global maximal yield. Consequently, the area of operating points in the liquidus projection can be divided into two adjoining areas by the operating line passing through the liquid phase belonging to the ternary eutectic equilibrium, i.e., the most diluted eutectic liquid phase of racemic composition (Figure 9). Any operating point on or below this line leads to the global maximal yield, whereas the ones above this line allow only for the local maximal yield. Hence, for a fixed ee_0, the optimal operating temperatures of the two classes of operating points yield two curves in the operating plane. As the two areas of operating points are adjacent, the two curves have a common point with coordinates corresponding to the optimal temperatures of the point located on the operating line dividing the two areas. The optimal final temperature of this point is always $T_{eut,solv-R-S}$ and corresponds to the lowest final temperature possible, whereas its optimal initial temperature is dependent on ee_0.

When considering conglomerate-forming systems exhibiting oiling out, the possible operating points lie on the two liquidus surfaces that are associated with the target enantiomer. In contrast to single conglomerate-forming systems, the liquidus projection features two regions consisting of possible operating points (pink areas in Figure 13). Independent of the type of system, each area is delimited by a monovariant eutectic curve through racemic liquid phases. The two curves stem from the intersections among the two upper and the two lower liquidus surfaces of the two enantiomers, respectively. Accordingly, each liquidus surface of the target enantiomer exhibits operating points that lead to the global maximal yield. The complete set of operating points of each liquidus surface can therefore be divided into two classes based on the maximal yield (Figure 14a and b).

The set of operating points on the upper liquidus surface is divided into two adjacent areas by the operating line through the solute-rich liquid phase of the ternary monotectic equilibrium, which is the most diluted racemic liquid phase, and is located on the upper liquidus surface. Operating points on or below this line lead to the global maximal yield, whereas the others lead to the local maximal yield. The optimal operating temperatures for a specific ee_0 value are therefore represented by two curves in the operating plane. Again the two regions of operating points are adjacent, and thus the two curves have one common point corresponding to the optimal operating temperatures of the operating point lying on the operating line dividing the two areas. The optimal final temperature of this point is always $T_{mon,L-R-S}$, whereas its optimal initial temperature depends on ee_0.

The area representing the set of operating points located on the lower liquidus surface is divided either into two or into three adjoining areas depending on the shape of the monovariant monotectic curve confining it.

In the case where no monotectic liquid phase allows maximizing the yield (Figure 14a), the two classes of operating points belong to two adjacent regions divided by the operating line passing through the liquid phase of the ternary eutectic equilibrium. As the area of operating points leading to the global maximal yield does not extend over the whole range of enantiomeric excesses, the global maximal yield is only obtained through operating points with an enantiomeric excess lower than ee* (ee* is defined as the enantiomeric excess of the intersection point among the operating line dividing the two regions and the projection of the monovariant monotectic curve confining the lower liquidus surface). Consequently, for ee_0 values below ee*, the operating points of the lower liquidus surface yield two curves of optimal operating temperatures in the operating plane, which have one common point. However for ee_0 values above ee*, no operating point located on the lower liquidus surface leads to the global maximal yield, thus the operating plane features only one curve, which represents the optimal operating temperatures leading to the local maximal yield.

In the case where monotectic liquid phases allow maximizing the yield, three different regions of operating points are obtained (Figure 14b). The region of operating points leading to the global maximal yield is adjacent to two areas representing operating points leading to the local maximal yield. Two operating lines divide the three regions, one passing through the liquid phase of the ternary eutectic equilibrium, the other through the solute-lean liquid phase belonging to the ternary monotectic equilibrium. The yield of operating points, which are more diluted than those leading to the global maximal yield, is maximized by obtaining equilibria involving eutectic liquid phases, whereas the yield of those which are more concentrated is maximized obtaining equilibria involving monotectic liquid phases. For any ee_0 value below ee′, operating points at constant initial enantiomeric enrichment yield three curves in the operating plane, two of them leading to the local maximal yield (ee′ is defined as the enantiomeric excess of the point of intersection between the operating line through the solute-lean liquid phase of the ternary monotectic curve and the projection of the monovariant monotectic curve confining the lower liquidus surface). The curve of operating temperatures leading to the global maximal yield has one point in common with each curve representing operating temperatures leading to the local maximal yield. Increasing the ee_0 value between ee′ and ee*, the operating points yield two curves, one curve through pairs of operating temperatures leading to the global maximal yield, the other through pairs of operating temperatures leading to the local maximum. Finally, for ee_0 values above ee*, the operating points yield only one curve in the operating plane representing optimal operating temperatures leading to the local maximal yield.

Independent of the type of system, the optimal final temperature for each operating point corresponds to the lowest final temperature that allows for the selective crystallization of the target enantiomer. Any final temperature below the optimal value will lead to the formation of an undesired phase. Therefore, the curves of optimal temperatures always delimit the region feasible for resolution from the unfeasible region.

The same methodology can also be applied to substances, which crystallize as a racemic compound. As the number of solid phases is increased by one, a new liquidus surface is introduced in the ternary phase diagram. The new liquidus surface intersects with the liquidus surfaces of the solvent and of the two enantiomers and, in the case of oiling out, also with the surface describing liquid−liquid phase equilibria. As temperatures exist where solid−liquid equilibria involving crystals of a pure enantiomer are thermodynamically stable, the selective crystallization of the desired enantiomer from enriched solutions is possible. Analogous to the conglomerate-forming systems, suitable operating points together with their pair of optimal operating temperatures can be determined. As the eutectic liquid phases maximizing the yield arise from the intersection between the liquidus surface of the racemic compound and of the target enantiomer, they are nonracemic and their enantiomeric excesses are generally dependent on temperature. Therefore, only one operating point out of the set of possible operating points at constant ee_0 will lead to the global maximal yield, whereas the others lead to a local maximal yield only.

5.2. Concluding Remarks about Practical Implementation. The design methodology presented here and based on the knowledge of the ternary phase diagram of the two enantiomers and the solvent allows determining for each initial enantiomeric excess a map of the operating regions in the plane having as coordinates the initial and the final crystallization temperature. Such a map contains one or more (in the case of oiling out) regions where chiral resolution of the target enantiomer can be achieved, and regions that are unfeasible in that respect.

Every region of chiral resolution is delimited by four lines, one of which consists of points when maximum yield is achieved. Each point along this optimal line corresponds to different initial and final temperature levels, hence different viscosity of the solution, different nucleation and growth rates, etc. High viscosity might make the postprocessing difficult. High growth rates might facilitate the formation of agglomerates and hence of inclusions of the wrong enantiomer into crystals of the target enantiomer. Temperature levels have of course also an impact not only on process costs but also on possible thermal degradation of the chiral compound. As a consequence, the choice of the operating temperatures along the optimal line shall be based on a careful trade-off between process costs and product quality.

On the other hand, there are reasons to choose an operating point not exactly on the optimal line but close to it within the region of chiral resolution. The optimal line depends on the phase diagram and on the initial enantiomeric excess. Any uncertainty on the phase diagram causes an uncertainty in the exact position of the optimal line in the operating plane. Unexpected changes in the performance of the upstream process might yield changes of the initial enantiomeric excess and as consequence a perturbation in the position of the optimal line. Accordingly any fluctuation in the operating temperatures might drive the operating point out of the optimal line even when this is known with the highest precision. In other words, operating points on the optimal line give the maximum yield at the cost of the minimum possible robustness, which is defined as the capacity of the system to withstand perturbations or uncertainties. Robustness can be improved by moving the operating point from the optimal line to a location within the region of chiral resolution. In practice this can be obtained by choosing a specific initial temperature and then by cooling the suspension to a temperature a few degrees above the optimal final temperature.

In conclusion, the design of a crystallization process to obtain pure crystals of the target enantiomer from an enriched solution requires that an optimal trade-off between yield and robustness be found. The knowledge of the phase diagram allows for the determination of the operating regions in the operating plane spanned by initial and final temperature, both in the case where no oiling out occurs and in that when it does. Such information provides a decisive support to the practitioner in search of such an optimal trade-off, as we are experiencing in running crystallization experiments with the chiral compound ethyl-2-ethoxy-3-(4-hydroxyphenyl)-propanoate, whose phase diagram has been previously reported.[17]

AUTHOR INFORMATION

Corresponding Author

*Phone: +41 44 632 24 56. Fax: +41 44 632 11 41. E-mail: marco.mazzotti@ipe.mavt.ethz.ch.

ACKNOWLEDGMENT

This work is a contribution to the research project INTENANT, funded by the European Commission within the seventh Framework Programme (project no. 214 129).

NOTATION

ee_0	enantiomeric excess of the feed solution
L	liquid phase
L_I	solute-lean phase in liquid−liquid phase region
L_{II}	solute-rich phase in liquid−liquid phase region
S_{solv}	crystals of the solvent
S_R	crystals of *R*-enantiomer
S_S	crystals of *S*-enantiomer
$T_{initial}$	initial temperature of the crystallization process
T_{final}	final temperature of the crystallization process
$T_{eut,R-S}$	temperature of the eutectic equilibrium $L \rightleftarrows S_R + S_S$
$T_{eut,solv-R}$	temperature of the eutectic equilibrium $L \rightleftarrows S_{solv} + S_R$
$T_{eut,solv-R-S}$	temperature of the eutectic equilibrium $L \rightleftarrows S_{solv} + S_R + S_S$
$T_{m,R}$	melting temperature of the *R*-enantiomer
$T_{m,solv}$	melting temperature of the solvent
$T_{mon,L-R}$	temperature of the monotectic equilibrium $L_I \rightleftarrows L_{II} + S_R$
$T_{mon,L-R-S}$	temperature of the monotectic equilibrium $L_I \rightleftarrows L_{II} + S_R + S_S$
$T_{uc,R}$	upper consolution temperature of the *R*-enantiomer/solvent system
$T_{uc,R-S}$	upper consolution temperature of the racemic mixture/solvent system
Y	yield of the crystallization process

REFERENCES

(1) Jones, M. J.; Aslund, B.; Bohlin, M.; Herschend, B. *Current and Future Challenges for Crystallization in the Pharmaceutical Industries*;

BIWIC 2009 16th International Workshop on Industrial Crystallization, Lappeenranta, Finland, 2009.
(2) Davies, N. M.; Teng, X. W. *Adv. Pharm.* **2003**, *1*, 242–252.
(3) Marchand, P.; Lefèbvre, L.; Querniard, F.; Cardinaël, P.; Perez, G.; J.-J., C.; G., C. *Tetrahedron: Asymmetry* **2004**, *15*, 2455–2465.
(4) Alvarez Rodrigo, A.; Lorenz, H.; Seidel-Morgenstern, A. *Chirality* **2004**, *16*, 499–508.
(5) Brenna, E.; Fuganti, C.; Gatti, F. G.; Parmeggiani, F. *Tetrahedron: Asymmetry* **2009**, *20*, 2594–2599.
(6) Lim, B. G.; Ching, C. B.; Tan, R. B. H.; Ng, S. C. *Chem. Eng. Sci.* **1995**, *50*, 2289–2298.
(7) Lorenz, H.; Sheehan, P.; Seidel-Morgenstern, A. *J. Chromatogr. A* **2001**, *908*, 201–214.
(8) Ströhlein, G.; Schulte, M.; Strube, J. *Sep. Sci. Technol.* **2003**, *38*, 3353–3383.
(9) Amanullah, M.; Mazzotti, M. *J. Chrom. A* **2006**, *1107*, 36–45.
(10) Rajendran, A.; Paredes, G.; Mazzotti, M. *J. Chrom. A* **2009**, *1216*, 709–738.
(11) Gou, L.; Robl, S.; Leonhard, K.; Lorenz, H.; Sordo, M.; Butka, A.; Kesselheim, S.; Wolff, M.; Seidel-Morgenstern, A.; Schaber, K. *Chirality* **2011**, *23*, 118–127.
(12) Worlitschek, J.; Bosco, M.; Huber, M.; Gramlich, V.; Mazzotti, M. *Helv. Chim. Acta* **2004**, *87*, 279–291.
(13) Perlberg, A. Studies on the Influence of the Counter Enantiomer on the Enantioselective Crystallization from Solution; Ph.D. Thesis, Otto-von-Guericke-Universität Magdeburg, Germany, 2006.
(14) Zhang, Y.; Mao, S.; Ray, A. K.; Rohani, S. *Cryst. Growth Des.* **2010**, *10*, 2879–2887.
(15) Fung, K. Y.; Ng, K. M. *Ind. Eng. Chem. Res.* **2005**, *2005*, 910–921.
(16) Kaspereit, M. Separation of Enantiomers by a Process Combination of Chromatography and Crystallisation; Ph.D. Thesis, Otto-von-Guericke-Universität Magdeburg, Germany, 2005.
(17) Codan, L.; Bäbler, M. U.; Mazzotti, M. *Cryst. Growth Des.* **2010**, *10*, 4005–4013.
(18) Deneau, E.; Steele, G. *Org. Process Res. Dev.* **2005**, *9*, 943–950.
(19) Lai, S. M.; Yuen, M. Y.; Siu, K. M.; Ng, L. K. S.; Wibowo, C. *AIChE J.* **2007**, *53*, 1608–1619.
(20) Veesler, S.; Lafferrère, L.; Garcia, E.; Hoff, C. *Org. Process Res. Dev.* **2003**, *7*, 983–989.
(21) Vogt, J. H. L. *J. Geol.* **1931**, *39*, 401–431.
(22) Prausnitz, J. M.; Lichtenthaler, R. N.; de Azevedo, E. G. *Molecular Thermodynamics of Fluid-Phase Equilibria*; Prentice Hall: Upper Saddle River, NJ, 1999.
(23) Gröbner, J.; Schmid-Fetzer, R. *JOM* **2005**, *57*, 19–23.
(24) Coquerel, G. *Top. Curr. Chem.* **2007**, *269*, 1–51.
(25) Wang, Y.; Chen, A. M. *Org. Process Res. Dev.* **2008**, *12*, 282–290.